Proceedings of the 1996 IEEE
International Conference on Robotics and Automation
Minneapolis, Minnesota - April 1996

Force Control of Constrained Flexible Manipulators

Jin-Soo Kim*, Kuniaki Suzuki*, Atsushi Konno** and Masaru Uchiyama*
*Department of Aeronautics and Space Engineering, Tohoku University
Aramaki-aza-Aoba, Aoba-ku, Sendai 980-77, Japan
** Department of Mechano-Informatics, University of Tokyo
Hongo 7-3-1, Bunkyo-ku, Tokyo 113, Japan

Abstract

In this paper, we discuss the force control of flexible manipulators. Since the force control of flexible manipulators with planar one or two links using the distributed-parameter modeling has been the subject of a considerable number of publications until now, so real time computations of the force control schemes are possible. But, application of those control schemes to multi-link spatial flexible manipulators is fairly complicated. In this paper, we apply a concise hybrid position/force control scheme to a flexible manipulator using a lumped-parameter modeling. The Hamilton's principle is applied to deriving the equations of motion and then, a state-space model is obtained by the Lagrange's method. Finally, a comparison between simulation and experimental results is presented to show the performance of our method.

1 Introduction

Because of the rapid development in industrial automation, high-speed and lightweight robots consuming less energy, are required. Moreover, in space applications, these properties are specially demanded. So, because of these requirements, in the past decade, a considerable number of researches have been devoted to the flexible manipulators, especially their modeling, vibration control, inverse kinematics and inverse dynamics. When a flexible manipulator is set to an environmental constraint, not only these algorithms but also force control algorithm is necessary to be implemented to complete the task. But so far, the publications about force control algorithms are not enough in number.

The research on force control of rigid manipulators began as early as 1960's but, the algorithm was systemized over 1970's to 1980's. The approaches developed are mainly divided into hybrid position/force control schemes and impedance control schemes [1], [2]. So, until now, force control of rigid manipulators has been one of the hottest research topics, however, the same for flexible manipulators just began in 1985 by Fukuda [3]. Chiou and Shahinpoor have pointed out that the link flexibility is the main cause of dynamic instability. They have extended their research from planar one-link flexible manipulator to two-link manipulator, analyzing their stability by applying hybrid position/force control schemes [4]. Matsuno and Yamamoto have addressed a quasi-static hybrid position/force control scheme and dynamic hybrid position/force control scheme for a planar two-DOF manipulator with flexible second link [5]. Kojima and Kawanabe have constructed the PIS control scheme which makes good use of the flexibility of robots, as without using any force sensor, the feedback of strain gauges has been used to control the contact force [6]. For force control of flexible manipulators, the inverse kinematic task is an essence, and has been proposed by Svinin and Uchiyama [7].

The above-mentioned researches have been mainly realized for only planar one-link or two-link flexible manipulators using distributed-parameter modeling. However, due to the complexity of distributed-parameter modeling, no attempts have been made for multi-link, multi-DOF spatial flexible manipulators. In some multi-link spatial flexible manipulators, equations of motion depend upon arm's configuration, and thus, real time computations are necessary, which are quite difficult and time consuming if distributed-parameter model is used, hence lumped-parameter model is effective for such purpose because of their simplicity [8].

Our aim is to develop the model for a constrained multi-link, multi-DOF spatial flexible manipulators, applying hybrid position/force control scheme to this model, and suppressing the vibrations in constrained conditions.

The equations of motion are obtained by applying the Hamilton's principle and the state-space model by the Lagrange's method. This model is analyzed on MATLAB. In the second step, a precise simulation model is developed using ADAMS^{TM}, which is a general purpose 3-dimensional analysis software. In order

0-7803-2988-4/96 $4.00 © 1996 IEEE

to simplify the discussions, we take the case of a 2-link manipulator moving in a vertical plane only.

Finally, experiments and simulations are performed, comparison of simulation results with experimental results is given to show the performance of our method.

2 Modeling of Constrained Flexible Manipulator

2.1 Constraint equation

The kinematic constraints stand for both nonintegrable nonholonomic and integrable holonomic constraints. The holonomic constraints are further divided into time-independent sceleronomous, and time-dependent rheonomous constraints [9]. In this paper, only rheonomous constraints are considered which can be written in the following form

$$\varphi(q,t)=0, \tag{1}$$

where $\varphi \in \Re^l$ are the linearly independent constraint equations, t is time, and q are the generalized coordinates.

2.2 Equations of motion

By using lumped-parameter model of the flexible manipulator, equations of motion can be derived by using Hamilton's principle, and can be written as

$$\begin{aligned}\begin{bmatrix}\tau\\0\end{bmatrix} &= \begin{bmatrix}M_{11}(q) & M_{12}(q)\\ M_{21}(q) & M_{22}(q)\end{bmatrix}\begin{bmatrix}\ddot{\theta}\\ \ddot{e}\end{bmatrix}\\ &+ \begin{bmatrix}h_1(q,\dot{q})\\ h_2(q,\dot{q})\end{bmatrix}+\begin{bmatrix}0 & 0\\ 0 & K_{22}\end{bmatrix}\begin{bmatrix}\theta\\ e\end{bmatrix}\\ &+ \begin{bmatrix}g_1(q)\\ g_2(q)\end{bmatrix}+\begin{bmatrix}J_{\varphi\theta}^T\lambda\\ J_{\varphi e}^T\lambda\end{bmatrix},\end{aligned} \tag{2}$$

or in a compact form

$$L\tau = M(q)\ddot{q}+h(q,\dot{q})+Kq+g(q)+J_\varphi^T\lambda, \tag{3}$$

where

$q=\begin{bmatrix}\theta\\ e\end{bmatrix}$: generalized coordinates,
$\theta \in \Re^n$ are the joint rotations,
$e \in \Re^m$ are the the elastic deflections,
τ : joint torques vector ($\Re^n$),
$M(q)$: inertia matrix,
$h(q,\dot{q})$: vector of centrifugal and Coriolis forces,
K : stiffness matrix,
$g(q)$: gravity vector,
J_φ : Jacobian matrix for constraints ($\Re^{l\times(n+m)}$),
λ : vector of Lagrange multiplier ($\Re^l$), and
L : transformation matrix,
$L=\begin{bmatrix} I_{n\times n}^T & 0_{m\times n}^T\end{bmatrix}^T$.

Jalón and Bayo have used the same constraint Jacobian matrix for both rheonomously and scleronomously constrained systems [9]. Therefore, here we can use Jacobian matrix for rheonomous constraints as

$$\begin{aligned}J_\varphi &= \frac{\partial\varphi}{\partial p}J_q(q)\\ &= \begin{bmatrix}\frac{\partial\varphi}{\partial\theta_1} & \frac{\partial\varphi}{\partial\theta_2} & \cdots\frac{\partial\varphi}{\partial\theta_n} & \frac{\partial\varphi}{\partial e_1} & \frac{\partial\varphi}{\partial e_2} & \cdots\frac{\partial\varphi}{\partial e_m}\end{bmatrix}\\ &= \begin{bmatrix}J_{\varphi\theta} & J_{\varphi e}\end{bmatrix},\end{aligned} \tag{4}$$

where $J_q=[J_\theta\ J_e]$ is standard Jacobian matrix of the manipulator, and p represents the Cartesian coordinates and the three Euler angles for the end-effector. Lagrange multiplier can be presented as

$$\begin{aligned}\lambda &= \frac{f_n}{|\mathrm{grad}\varphi|},\\ \mathrm{grad}\varphi &= \nabla\varphi=\frac{\partial\varphi}{\partial p},\end{aligned} \tag{5}$$

where f_n is the component of contact force normal to the constraints.

In order to simplify Eqs. (2) and (3), we make the following assumptions:

- Only the slow motion is considered, and thus the centrifugal and Corioli's forces can be neglected,
$$h(q,\dot{q})=0,$$
- The influence of elastic deflections e is supposed to be small, and thus,
$$M(\theta,e)\approx M(\theta),\quad g(\theta,e)\approx g(\theta).$$

In the stationary condition (i.e., $\ddot{\theta}=\dot{\theta}=0$ and $\ddot{e}=\dot{e}=0$), Eq. (2) becomes

$$\begin{aligned}\begin{bmatrix}\tau_0\\0\end{bmatrix} &= \begin{bmatrix}0 & 0\\ 0 & K_{22}\end{bmatrix}\begin{bmatrix}\theta_0\\ e_0\end{bmatrix}\\ &+ \begin{bmatrix}g_1(\theta_0)\\ g_2(\theta_0)\end{bmatrix}+\begin{bmatrix}J_{\varphi\theta}^T\lambda_0\\ J_{\varphi e}^T\lambda_0\end{bmatrix},\end{aligned} \tag{6}$$

where τ_0 are the static torques to keep the arm in a configuration to balance the gravity and contact force, e_0 are the static deflections due to gravity and contact forces, and θ_0, λ_0 are respectively the angles and the Lagrange multipliers for the static condition. In addition, Δe , $\Delta\tau$, $\Delta\theta$ and $\Delta\lambda$ can be respectively expressed as follows:

$$\begin{aligned}\Delta\tau &= \tau-\tau_0=\tau-(g_1(\theta_0)+J_{\varphi\theta}^T\lambda_0),\\ \Delta e &= e-e_0=e+K_{22}^{-1}(g_2(\theta_0)+J_{\varphi e}^T\lambda_0),\\ \Delta\theta &= \theta-\theta_0,\\ \Delta\lambda &= \lambda-\lambda_0.\end{aligned} \tag{7}$$

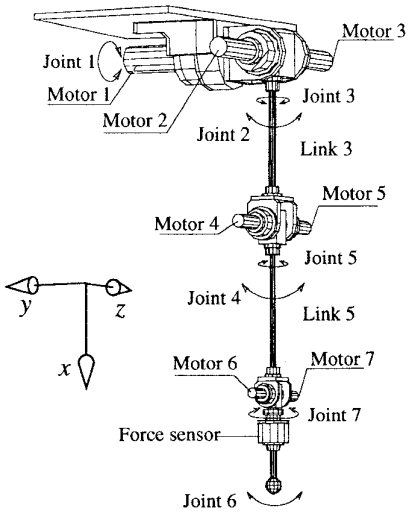

Figure 1: Experimental robot with 2 links and 7 joints.

Incorporating Eq. (7) along with above assumptions into Eq. (2), the compact form is achieved as

$$\boldsymbol{L}\Delta\boldsymbol{\tau} = \boldsymbol{M}(\theta)\Delta\ddot{\boldsymbol{q}} + \boldsymbol{K}\Delta\boldsymbol{q} + \boldsymbol{J}_{\varphi}^{T}\Delta\boldsymbol{\lambda}, \tag{8}$$

where $\Delta\boldsymbol{q} = \left[\begin{array}{cc} \Delta\boldsymbol{\theta}^T & \Delta\boldsymbol{e}^T \end{array}\right]^T$. The constraint environment is modeled as a spring with a large spring constant, therefore Lagrange multiplier $\Delta\boldsymbol{\lambda}$ is given by

$$\begin{aligned} \Delta\boldsymbol{\lambda} &= \boldsymbol{K}_{env}\boldsymbol{N}\Delta\boldsymbol{p} \\ &= \boldsymbol{K}_{env}\boldsymbol{N}(\boldsymbol{J}_{\theta}\Delta\boldsymbol{\theta} + \boldsymbol{J}_{e}\Delta\boldsymbol{e}), \end{aligned} \tag{9}$$

where $\boldsymbol{K}_{env}$ are the environmental stiffnesses, $\Delta\boldsymbol{p}$ are the deflections of the constraints, $\boldsymbol{n} = \frac{\nabla\varphi}{|\nabla\varphi|}$ are the unit vector normal to the constraints, and $\boldsymbol{N} = \boldsymbol{n}^T\boldsymbol{n}$.

Substituting Eq. (9) into Eq. (8), the approximated equations of motion can be written as

$$\begin{aligned} \left[\begin{array}{c} \Delta\boldsymbol{\tau} \\ \boldsymbol{0} \end{array}\right] &= \left[\begin{array}{cc} \boldsymbol{M}_{11}(\theta) & \boldsymbol{M}_{12}(\theta) \\ \boldsymbol{M}_{21}(\theta) & \boldsymbol{M}_{22}(\theta) \end{array}\right] \left[\begin{array}{c} \Delta\ddot{\boldsymbol{\theta}} \\ \Delta\ddot{\boldsymbol{e}} \end{array}\right] + \\ &\left[\begin{array}{cc} \boldsymbol{J}_{\varphi\theta}^{T}\boldsymbol{K}_{env}\boldsymbol{N}\boldsymbol{J}_{\theta} & \boldsymbol{J}_{\varphi\theta}^{T}\boldsymbol{K}_{env}\boldsymbol{N}\boldsymbol{J}_{e} \\ \boldsymbol{J}_{\varphi e}^{T}\boldsymbol{K}_{env}\boldsymbol{N}\boldsymbol{J}_{\theta} & \boldsymbol{K}_{22} + \boldsymbol{J}_{\varphi e}^{T}\boldsymbol{K}_{env}\boldsymbol{N}\boldsymbol{J}_{e} \end{array}\right] \left[\begin{array}{c} \Delta\boldsymbol{\theta} \\ \Delta\boldsymbol{e} \end{array}\right], \end{aligned} \tag{10}$$

or in a more compact form

$$\boldsymbol{L}\Delta\boldsymbol{\tau} = \boldsymbol{M}(\boldsymbol{\theta})\Delta\ddot{\boldsymbol{q}} + \boldsymbol{K}^{*}\Delta\boldsymbol{q}. \tag{11}$$

3 Simulations and Experiment

To clarify the discussion, the motions of an experimental flexible manipulator ADAM (Aerospace Dual Arm Manipulator) are considered. ADAM has two arms and each arm consists of 2 elastic links and 7 rotary joints [10]. In this paper, however, only the left arm of ADAM (Fig. 1) is considered. The discussion is restricted to only the vertical motion of joints 2, 4 and 6 (θ_2, θ_4, θ_6) while joint 6 always preserves an angle of $\pi/2$ [rad] with respect to constraints.

Table 1: ADAM link parameters.

	Link 3	Link 5
Length	0.5 m	0.5 m
Elastic part	0.359 m	0.394 m
Diameter	0.013 m	0.01 m
Material	SUP-6	SUP-6
EI	288.1 Nm^2	100.8 Nm^2
Mass	0.7 kg	0.5 kg

Based on the above model, two simulations are performed. The results, achieved by a precise model constructed by commercial dynamic analysis software packages, are compared with experimental results.

3.1 Experimental setup

The experimental manipulator ADAM is driven by DC servo motors with hardware velocity control. Each of motors 1-3 has an optical encoder for sensing the joint angle and a tachometer for sensing the angular velocity. None of the motors 4-7 has a tachometer, and thus, pulse signals generated by optical encoder are translated into velocity signals through F/V (Frequency to Voltage) converter.

The parameters of each link of ADAM are presented in Table 1. Strain gauges are used to measure the link vibrations while a force sensor is used to measure the contact force at end-effector.

3.2 A lumped-mass spring model

The arm under consideration is modeled by lumped-masses and massless springs as shown in Fig. 2. The lumped masses are considered concentrated at the tip of respective links while the links are considered as massless springs with elastic and torsional properties as E_3I_3, E_5I_5 and G_3J_3, G_5J_5, respectively.

3.3 Control scheme

We shall make use of a simple control scheme which represents our initial approach to the sophisticated control problem. More details on the control, such as stability analysis, will be presented elsewhere.

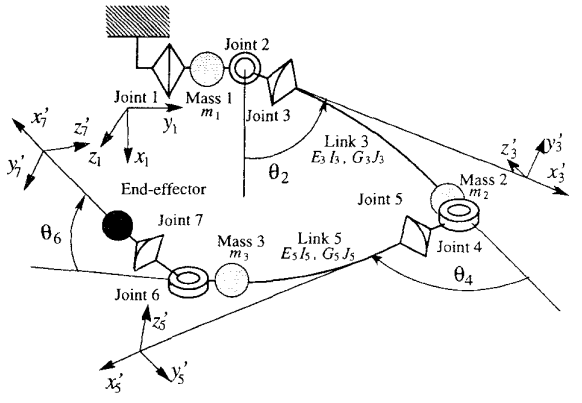

Figure 2: Lumped-parameter model of the experimental manipulator ADAM.

As ADAM is equipped with the velocity feedback servo motors, so joint motion is commanded by joint velocity command, and therefore joint torque cannot be controlled directly. Hence, we assume the relationship between velocity command and the produced torque as follows

$$\begin{aligned} \boldsymbol{\tau} &= \boldsymbol{G}_r \boldsymbol{K}_{sp}(\boldsymbol{V}_{ref} - \boldsymbol{K}_{sv}\dot{\boldsymbol{\theta}}_m), \\ &= \boldsymbol{\Lambda}(\dot{\boldsymbol{\theta}}_c - \dot{\boldsymbol{\theta}}), \end{aligned} \tag{12}$$

where

$\boldsymbol{G}_r$	:	gear reduction ratios,
$\boldsymbol{K}_{sp}$	:	voltage feedback gains,
$\boldsymbol{K}_{sv}$	:	voltage/velocity coefficients,
$\dot{\boldsymbol{\theta}}_m = \boldsymbol{G}_r\dot{\boldsymbol{\theta}}$	:	angular velocities of motors,
$\boldsymbol{V}_{ref}$	:	voltage velocity commands,
$\dot{\boldsymbol{\theta}}_c$	:	velocity commands, and
$\boldsymbol{\Lambda} = {\boldsymbol{G}_r}^2\boldsymbol{K}_{sp}\boldsymbol{K}_{sv}$	:	velocity feedback gains.

Voltage velocity commands $\boldsymbol{V}_{ref}$ are computed by

$$\boldsymbol{V}_{ref} = \boldsymbol{G}_r\boldsymbol{K}_{sv}\dot{\boldsymbol{\theta}}_c, \tag{13}$$

and are used in the experiments.

As we can see, from Eq. (6), that the elastic deflection are dependent upon the contact forces when the manipulator moves slowly enough. So the vibration of manipulator can be suppressed by controlling the contact forces. The approximate joint velocities $\dot{\boldsymbol{\theta}}_c$ can be computed as follows

$$\dot{\boldsymbol{\theta}}_c = \dot{\boldsymbol{\theta}}_t + \dot{\boldsymbol{\theta}}_f, \tag{14}$$

where $\dot{\boldsymbol{\theta}}_t$ is the joint velocity vector for positioning while $\dot{\boldsymbol{\theta}}_f$ are the additional factor for force control. The velocities $\dot{\boldsymbol{\theta}}_t$ and $\dot{\boldsymbol{\theta}}_f$ are respectively computed as

$$\begin{aligned} \dot{\boldsymbol{\theta}}_t &= \boldsymbol{J}_{\theta}^{-1}(\boldsymbol{I} - \boldsymbol{n}^T\boldsymbol{n})\boldsymbol{K}_{tp}(\boldsymbol{p}_d - \boldsymbol{p}), \\ \dot{\boldsymbol{\theta}}_f &= \boldsymbol{\Lambda}^{-1}\boldsymbol{J}_{\theta}^T\boldsymbol{n}^T K_{fp}(\lambda_d - \lambda), \end{aligned} \tag{15}$$

where $\boldsymbol{I}$ is unit matrix. $\boldsymbol{n}^T$, $(\boldsymbol{I} - \boldsymbol{n}^T\boldsymbol{n})$ define matrices which respectively select force and position directions. $\boldsymbol{K}_{tp}$ is a proportional gain matrix for positioning while K_{fp} is a proportional gain scalar for force control.

From Eqs. (7) and (12) we have

$$\Delta\boldsymbol{\tau} = \boldsymbol{\Lambda}\{(\dot{\boldsymbol{\theta}}_c - \dot{\boldsymbol{\theta}}) - \boldsymbol{\Lambda}^{-1}(\boldsymbol{g}_1(\boldsymbol{\theta}_0) + \boldsymbol{J}_{\varphi\theta}^T\boldsymbol{\lambda}_0)\}. \tag{16}$$

If the velocity servo loop is sufficiently stiff, that is, the gains $\boldsymbol{\Lambda}$ are high, the term $\boldsymbol{\Lambda}^{-1}(\boldsymbol{g}_1(\boldsymbol{\theta}_0) + \boldsymbol{J}_{\varphi\theta}^T\boldsymbol{\lambda}_0)$ can be neglected. Eq. (16) can be represented as follows

$$\begin{aligned} \Delta\boldsymbol{\tau} &= \boldsymbol{\Lambda}\{(\dot{\boldsymbol{\theta}}_c - \dot{\boldsymbol{\theta}}_0) - \{(\dot{\boldsymbol{\theta}} - \dot{\boldsymbol{\theta}}_0)\} \\ &= \boldsymbol{\Lambda}(\Delta\dot{\boldsymbol{\theta}}_c - \Delta\dot{\boldsymbol{\theta}}). \end{aligned} \tag{17}$$

Then, substituting Eq. (17) into Eq. (11) and taking into account the fact that $\Delta\dot{\boldsymbol{\theta}} = \boldsymbol{L}^t\Delta\dot{\boldsymbol{q}}$, the equations of motion of constrained flexible manipulator are obtained as

$$\boldsymbol{M}\Delta\ddot{\boldsymbol{q}} + \boldsymbol{L}\boldsymbol{\Lambda}\boldsymbol{L}^T\Delta\dot{\boldsymbol{q}} + \boldsymbol{K}^*\Delta\boldsymbol{q} = \boldsymbol{L}\boldsymbol{\Lambda}\Delta\dot{\boldsymbol{\theta}}_c. \tag{18}$$

Eq. (18) can be transformed into the state space form as

$$\begin{aligned} \begin{bmatrix} \Delta\ddot{\boldsymbol{q}} \\ \Delta\dot{\boldsymbol{q}} \end{bmatrix} &= \begin{bmatrix} -\boldsymbol{M}^{-1}\boldsymbol{L}\boldsymbol{\Lambda}\boldsymbol{L}^T & -\boldsymbol{M}^{-1}\boldsymbol{K}^* \\ \boldsymbol{I} & \boldsymbol{0} \end{bmatrix} \\ &\times \begin{bmatrix} \Delta\dot{\boldsymbol{q}} \\ \Delta\boldsymbol{q} \end{bmatrix} + \begin{bmatrix} \boldsymbol{M}^{-1}\boldsymbol{L}\boldsymbol{\Lambda} \\ \boldsymbol{0} \end{bmatrix}\Delta\dot{\boldsymbol{\theta}}_c, \end{aligned} \tag{19}$$

Eq. (19) can be cast into state space equation form as follows

$$\Delta\dot{\boldsymbol{x}} = \boldsymbol{A}\Delta\boldsymbol{x} + \boldsymbol{B}\Delta\dot{\boldsymbol{\theta}}_c. \tag{20}$$

In the simulations, the discrete-time state equation corresponding to Eq. (20) is used in the following form

$$\Delta\boldsymbol{x}(k+1) = \boldsymbol{\Phi}\Delta\boldsymbol{x}(k) + \boldsymbol{\Gamma}\Delta\dot{\boldsymbol{\theta}}_c(k), \tag{21}$$

where k indicates the k-th interval of the sampling process, $\boldsymbol{\Phi}$ and $\boldsymbol{\Gamma}$ are the discrete matrices of $\boldsymbol{A}$ and $\boldsymbol{B}$ for a zero-order holder (ZOH).

3.4 A precise model

A precise model of the ADAM robot is constructed by ADAMS^{TM}. ADAMS^{TM} is a commercial software package for dynamic analysis of mechanical systems produced by Mechanical Dynamics, Inc. In this simulator, a finite-element method based on Timosenko beam theory is used as a modeling method for flexible structures. To obtain a precise model, the elastic beam is divided into five pieces.

3.5 Results and discussion

We present the experimental and simulations results for the case when end-effector is not moving, and when it is moving while applying force. The constraint is a vertical plane located at 0.375 [m] in the y direction from the robot's reference coordinates. So, the end-effector is constrained in only the y direction, whereas it is free to move in the $x-z$ plane. In the second case, end-effector moves with a velocity of 0.17 [m/s] and the desired contact force of 5 [N].

The responses of task motion and contact force at the tip, as achieved by simulations and experiments, are shown in **Fig. 3** and **Fig. 4**, respectively. In **Fig. 3**, $\boldsymbol{K}_{tp} = \mathrm{diag}[1\ 1]$ [rad/(m s)] and $K_{fp} = 0.2$ [rad/(N s)], and in **Fig. 4**, $\boldsymbol{K}_{tp} = \mathrm{diag}[4\ 4]$ [rad/m s] and $K_{fp} = 0.4$ [rad/(N s)]. The sampling time is set as 10 [ms], and for these simulations, K_{sp} of Eq. (12) is decided to be approximated to the experimental results, and the environmental stiffness is taken as 5000 [N/m]. In **Fig. 3** and **Fig. 4**, "ADAMS" stands for ADAMS simulation software while "MATLAB" stands for MATLAB simulation software.

Fig. 3 and **Fig. 4** show that the presented control scheme, which does not consider the vibration control, is effective for constrained flexible manipulators modeled by lumped-parameter modeling method. In case of free motion of end-effector, the vibration suppression is necessary for position control, however, in case of constrained motion of end-effector, elastic deflection of link is constrained in the force control direction, so application of vibration control scheme is not necessary due to dependency between elastic deflection of link and the contact force. So, vibrations for constrained flexible manipulators are automatically suppressed by controlling the contact force.

4 Conclusions

A hybrid position/force control scheme for flexible manipulators has been presented. Experimental results show that the system responses are in good agreement with simulation results. Investigating these results, it can be concluded that our control scheme is effective.

Until now, the force control scheme of rigid manipulators has been passively applied to flexible manipulators, however, the future work in this area may find the active application of elastic deflection and compliance of the links to force control of flexible manipulators. In that case, the important relation between force and elastic deflection for even slow motion of flexible manipulators can also be applied to force control.

References

[1] M. H. Raibert and J. J. Craig, "Hybrid position/force control of manipulators," *Trans. ASME, J. of Dynamic System, Measurement and Control*, vol. 103, no. 2, pp. 126–133, 1981.

[2] M. T. Mason, "Compliance and force control for computer controlled manipulators," *IEEE Trans. on Systems, Man and Cybernetics*, vol. SMC-11, pp. 418–432 1981.

[3] T. Fukuda, "Flexibility control of elastic robotic arms," *J. Robotic Systems*, vol. 2, no. 1, pp. 73–88, 1985.

[4] B. C. Chiou and M. Shahinpoor, "Dynamics Stability Analysis of a One-Link Force-Controlled Flexible Manipulator," *J. Robotic Systems*, vol. 5, no. 5, pp. 443–451, 1988.

[5] F. Matsuno and K. Yamamoto, "Dynamic Hybrid Position/Force Control of a Flexible Manipulator, " *Proc. of the IEEE Int. Conf. on Robotics and Automation*, vol. 2, pp. 462–467, 1993.

[6] H. Kojima and T. Kawanabe, "Position and Force Control of Flexible Robot Arm with PIS Control," *J. Robotics Society of Japan*, vol. 10, no. 3, pp. 353–360, 1992 (in Japanese).

[7] M. M. Svinin and M. Uchiyama, "Contribution to Inverse Kinematics of Flexible Robot Arm," *Int. J. JSME, Series C*, vol. 37, no. 4, pp. 755–764, 1994.

[8] A. Konno and M. Uchiyama, "Modeling of a Flexible Manipulator Dynamics Based on the Holzer's Method," *J. Robotics Society of Japan*, vol. 12, no. 7,pp. 1021–1028, 1994 (in Japanese).

[9] J. G. Jalón and E. Bayo, Kinematic and Dynamic Simulation of Multibody System, *Springer-Verlag New York*, 1994.

[10] M. Uchiyama, A. Konno, T. Uchiyama, and S. Kanda, "Development of a flexible dual-arm manipulator testbed for space robotics," *Proc. of the IEEE Int. Workshop on Intelligent Robotics and Systems'90*, pp. 375–381, Tsuchiura, Japan, 1990.

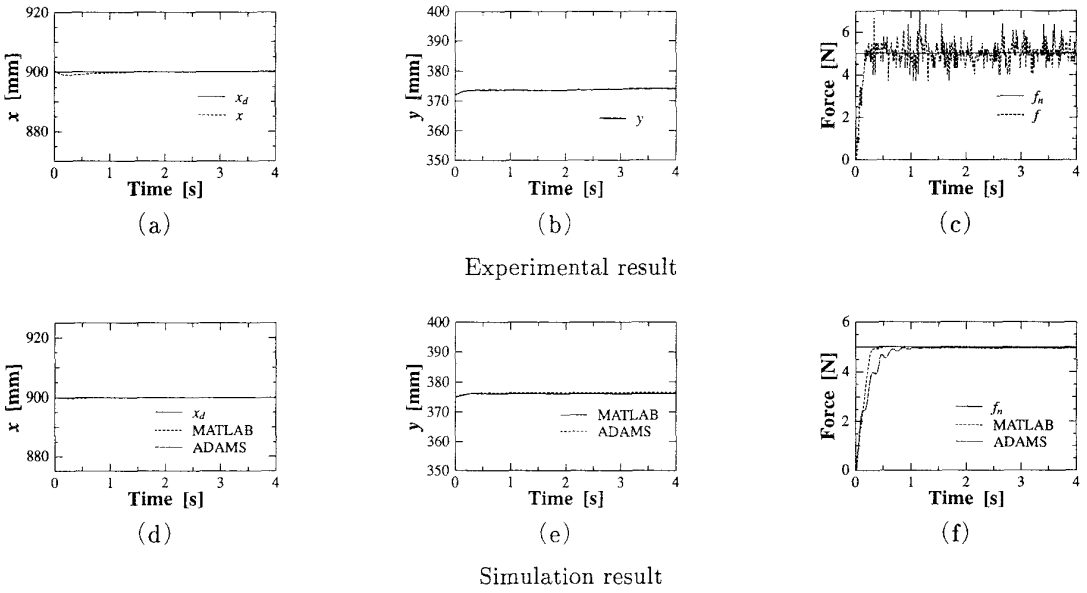

Figure 3: When end-effector of robot arm does not move.

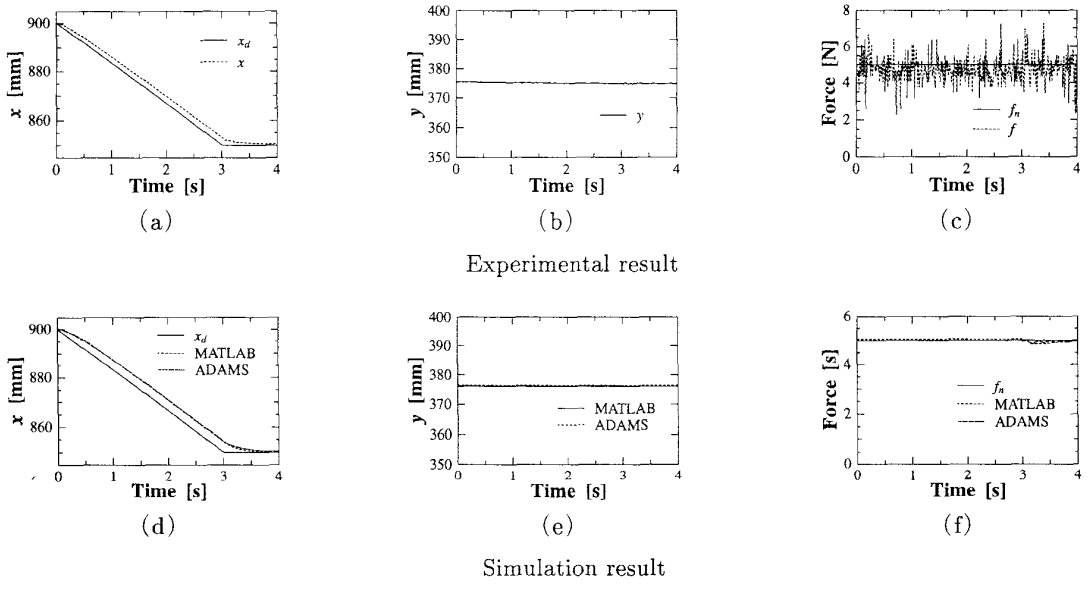

Figure 4: When end-effector of robot arm moves.